DOI: 10.6919/ICJE.202510_11(10).0006

Impact of Venturi-Effect Turbine Arrangements on Total Power Generation

Keming Gong

Shenzhen College of International Education, Shenzhen, Guangdong, 518048, China

Abstract

Venturi ducts accelerate incoming flows through geometric contraction and thereby enhance the power output of individual hydro-turbines. Nevertheless, when multiple turbines operate in an array, wake effects can substantially re-duce the overall efficiency, making the layout a critical factor in plant performance. In this study, two-dimensional computational fluid dynamics simulations were conducted to compare the flow fields and aggregate power of five Venturi-assisted turbines arranged in either a straight line or a staggered configuration. Moreover, the influence of tail-to-head spacing (8.67, 10.00, and 11.33 m) was systematically examined. The results demonstrate that, in the straightline lay-out, the centerline velocity of downstream turbines decreases by approximately 75% relative to the upstream turbine, yielding only a marginal increase in total power (from 6.55 kW to 6.73 kW). By contrast, the staggered layout generates inter-row acceleration corridors, leading to inflow velocities higher than the free stream for all turbines, while the total power decreases as spacing increases (from 47.19 kW to 44.01 kW). Overall, the staggered arrangement delivers nearly sevenfold higher total power ($\approx 701\%$) compared with the straight-line case. These findings highlight that staggered configurations with controlled inter-row spacing are essential for maximizing the efficiency of Venturi-turbine arrays, thereby providing theoretical guidance for the design of underwater power plants.

Keywords

Venturi Effect Turbine; Turbine Array Layout; Wake Effects; Staggered Configuration; CFD.

1. Introduction

A Venturi tube is composed of a contraction section, a throat, and a diffusion section. When the fluid passes through the throat, the reduced cross-sectional area accelerates the flow and simultaneously lowers the pressure, which is known as the Venturi effect. Because of its high energy efficiency, simple structure, and scalability, this effect has been widely applied in engineering and energy systems, such as flow measurement, natural gas transmission, internal combustion engine pressurization, and industrial waste-gas cleaning^{[1][2][3]}. In process industries and environmental engineering, studies on hydrodynamic cavitation have shown that the low-pressure region and shear induced by Venturi geometries can promote microbubble generation and mass transfer, which enhances mixing and chemical reactions. This mechanism has demonstrated potential in mineral flotation, wastewater treatment, food processing, and reaction intensification ^{[4][5][6][7][8][9]}. Overall, understanding the velocity and pressure distribution inside Venturi tubes, and optimizing the geometry and operating conditions accordingly, is of great significance for improving energy utilization efficiency and expanding industrial applications ^{[10][11]}.

DOI: 10.6919/ICJE.202510_11(10).0006

In recent years, both experimental and numerical studies have investigated the influence of Venturi geometric parameters on internal flow and cavitation characteristics. Parameters such as contraction ratio, throat length-to-diameter ratio, diffusion angle, and outlet-to-throat diameter ratio have been found to significantly affect local pressure distribution, cavitation inception, microbubble generation, overall pressure loss, and mass flux^{[3][12][13][14][15][16]}. For instance, an increase in diffusion angle can raise the mass flux, although it may also induce asymmetric flow patterns and additional losses, while an excessive contraction ratio leads to a significant rise in pressure loss^{[3][14][15]}. In the field of hydrokinetic energy utilization, Venturi ducts have been introduced as contraction-expansion passages that accelerate the inflow upstream of the rotor, thereby increasing turbine in-let velocity and power output. This design approach is consistent with the research trend on diffuser-augmented or Venturi-assisted turbines^[17]. Nevertheless, when multiple turbines are deployed in arrays, inevitable wake interactions reduce downstream inflow velocity and increase turbulence, which ultimately diminishes plant-level efficiency. Previous studies on arrays and wake interactions have indicated that appropriate staggered layouts and optimized spacing between rows can shorten wake recovery distances, form acceleration corridors, and consequently improve the overall energy yield of the array^{[18][19]}.

Although the influence of Venturi geometry on single-turbine performance has been well documented [13][15][20], systematic comparisons of array configurations for Venturi-assisted hydrokinetic turbines remain limited. In particular, the differences between straight-line and staggered layouts in wake mitigation and flow redistribution have not been thoroughly addressed, and the quantitative influence of tail-to-head spacing on total power output and centerline velocity has not been clearly established. To address this gap, the present study employs the lattice Boltzmann method to simulate the flow and power performance of five Venturi-effect turbines arranged in straight-line and staggered configurations, while systematically examining the sensitivity of array performance to tail-to-head spacing. The results reveal that in straight-line layouts, upstream and downstream turbines form a "velocity reduction chain," which allows only a slow increase in total power as spacing grows. In contrast, staggered layouts generate stable acceleration corridors between rows, ensuring higher downstream inflow velocities and leading to a substantial rise in total power. These findings provide both physical insights and quantitative evidence for optimizing the layout of Venturi-assisted hydrokinetic arrays, and they also offer theoretical guidance for the engineering design of distributed underwater power plants [17][18][19].

2. Description of the Computational Setup

As shown in Figs. 1 and 2, the computational domain consists of five identical Venturi-effect turbines arranged in two typical configurations: a straight-line layout and a staggered layout. In the straight-line case, all turbines are aligned along the same centerline, and the tail-to-head spacing between successive units is denoted as D. In the staggered case, the second row is vertically shifted by half of the row spacing relative to the first row, forming an alternating pattern. By varying D (8.666660 m, 9.999948 m, and 11.333288 m), the effects of array layout and spacing on wake development and total power output can be systematically examined.

For the numerical simulations, the inlet boundary is specified as a velocity inlet with a constant free-stream velocity, while the outlet is prescribed as a pressure outlet with velocity gradients set to zero in order to prevent non-physical reflections. The upper and lower boundaries of the domain also employ zero-gradient conditions to approximate an open flow $(\partial u/\partial n = \partial v/\partial n = 0)$. The walls of the Venturi passages satisfy no-slip conditions, meaning the fluid velocity at the solid boundary is set to zero to capture boundary-layer formation. All cases are simulated under identical boundary conditions, with only the turbine layout and the tail-to-head spacing being varied. At the macroscopic scale, the flow field is governed by the two-dimensional incompressible Navier–Stokes equations, which can be written in vector form as

DOI: 10.6919/ICJE.202510_11(10).0006

$$\nabla \cdot \mathbf{u} = 0 \tag{1}$$

$$\rho \left(\frac{\partial u}{\partial t} + (u \cdot \nabla)u \right) = -\nabla p + \mu \nabla^2 u + \rho \vec{g}$$
 (2)

$$\frac{\partial(\rho k)}{\partial t} + \frac{\partial(\rho u_j k)}{\partial x_j} = \frac{\partial}{\partial x_j} \left[\left(\mu + \frac{\mu_t}{\sigma_k} \right) \frac{\partial k}{\partial x_j} \right] + P_k - \rho \varepsilon \tag{3}$$

$$\frac{\partial(\rho\varepsilon)}{\partial t} + \frac{\partial(\rho u_j\varepsilon)}{\partial x_j} = \frac{\partial}{\partial x_j} \left[\left(\mu + \frac{\mu_t}{\sigma_\varepsilon} \right) \frac{\partial\varepsilon}{\partial x_j} \right] + C_{1\varepsilon} \frac{\varepsilon}{k} P_k - C_{2\varepsilon} \rho \frac{\varepsilon^2}{k}$$
(4)



Fig. 1 Straight-Line Arrangement



Fig. 2 Alternating Arrangement

In addition to the arrangement of turbines, the geometry of the Venturi tunnel also plays a crucial role in determining the power extraction. Following the relationship proposed by Jung et al.^[21], the acceleration ratio of the Venturi passage can be approximated as

$$\frac{V_t}{V_{\infty}} = 2.03 - 0.95R_A,\tag{5}$$

where R_A denotes the area ratio between the throat cross-section and the inlet. Knowing that the power output of a turbine can be expressed as

DOI: 10.6919/ICJE.202510_11(10).0006

$$P = 0.5\rho A u^3,\tag{6}$$

the power of a Venturi-effect turbine can therefore be written as

$$P_{output} = 0.5\rho A R_A (2.03 - 0.95 R_A)^3 u_{\infty}.$$
 (7)

By keeping the fluid density, inlet area, and free-stream velocity constant, this equation can be simplified to

$$P_{output} \propto R_A (2.03 - 0.95R_A)^3.$$
 (8)

3. Method

3.1 Lattice Boltzmann Model

The lattice Boltzmann method (LBM) can be categorized into three major models depending on the choice of collision operator: the single relaxation time (SRT) model, also known as the Bhatnagar–Gross–Krook (BGK) model, the two relaxation time (TRT) model, and the multiple relaxation time (MRT) model. Owing to its simplicity and efficiency, the SRT model is widely ap-plied in incompressible flow simulations. Since the present study focuses on two-dimensional incompressible flow at moderate Reynolds numbers, the SRT model is adopted to capture the flow dynamics of Venturi-effect turbine arrays. In the BGK framework, the evolution of the particle distribution function f_i (X, t) is governed by

$$f_i(\mathbf{x} + \mathbf{c}_i \Delta t, t + \Delta t) - f_i(\mathbf{x}, t) = -\frac{1}{\tau} \left[f_i(\mathbf{x}, t) - f_i^{eq}(\mathbf{x}, t) \right], \tag{9}$$

where c_i denotes the discrete lattice velocity, \mathcal{T} is the relaxation time, and f_i^{eq} is the equilibrium distribution function. To ensure numerical accuracy while maintaining computational efficiency, the two-dimensional nine-velocity (D2Q9) lattice model is employed in this work. The equilibrium distribution function is constructed by a second-order expansion of the Maxwell-Boltzmann distribution, and is given as

$$f_i^{eq} = w_i \rho \left[1 + \frac{\mathbf{c}_i \cdot \mathbf{u}}{c_s^2} + \frac{(\mathbf{c}_i \cdot \mathbf{u})^2}{2c_s^4} - \frac{|\mathbf{u}|^2}{2c_s^2} \right],\tag{10}$$

where ρ is the fluid density, **u** is the macroscopic velocity, $c_s = c/\sqrt{3}$ is the lattice speed of sound, and w_i are the lattice weights with values $w_0 = 4/9$, $w_{1-4} = 1/9$, and $w_{5-8} = 1/36$. Based on the statistical moments of the distribution functions, the macroscopic flow variables are recovered as

DOI: 10.6919/ICJE.202510_11(10).0006

$$\rho = \sum_{i} f_i, \rho \mathbf{u} = \sum_{i} \mathbf{c}_i f_i, \tag{11}$$

Furthermore, the fluid viscosity is linked to the relaxation parameter by

$$\nu = c_s^2 \left(\tau - \frac{1}{2}\right) \Delta t. \tag{12}$$

3.2 Boundary Condition

In the lattice Boltzmann framework, boundary treatment plays a crucial role in ensuring numerical stability and physical accuracy. In this work, two classical schemes are adopted. For the solid walls of the Venturi passages, the standard bounce-back scheme is employed to enforce the no-slip condition. When a particle distribution function f_i hits the boundary, it is instantaneously reflected back along the opposite direction:

$$f_i(\mathbf{x}_f, t + \Delta t) = f_{\bar{i}}(\mathbf{x}_f, t), \tag{13}$$

where \mathbf{x}_f denotes the boundary node location, and i and \bar{i} are a pair of opposite lattice directions. This ensures that the macroscopic velocity at the wall is zero, thereby satisfying the no-slip condition. At the inlet and outlet boundaries, the non-equilibrium extrapolation scheme is applied to maintain numerical stability. In this approach, the distribution function is decomposed into its equilibrium and non-equilibrium parts:

$$f_i = f_i^{eq}(\rho, \mathbf{u}_b) + \left[f_i(\mathbf{x}_f, t) - f_i^{eq}(\rho, \mathbf{u}_f) \right], \tag{14}$$

where \mathbf{u}_b is the prescribed boundary velocity (known at the inlet or computed from the outlet pressure), and \mathbf{u}_f is the velocity at the fluid node adjacent to the boundary. This method effectively avoids non-physical reflections and ensures continuity between the boundary and the interior flow field.

Through this treatment, the bounce-back scheme is used to model solid walls with no-slip conditions, while the non-equilibrium extrapolation scheme is adopted at inlets and outlets to allow consistent inflow and outflow, thereby guaranteeing the accuracy and robustness of the simulations.

4. Results and Discussion

We present a comparative analysis of the performance of Venturi-effect turbines under different array configurations. Specifically, we first investigate the influence of wake effects in the straight-line arrangement, which significantly reduces the inflow velocity and power output of downstream turbines. We then examine the staggered arrangement, in which the offset placement of turbines generates accelerated flow channels that enhance downstream performance and improve the total power output of the array. Finally, the impact of varying tail-to-head spacing is analyzed to reveal the coupled relationship between array spacing and overall energy extraction efficiency. The velocity fields and power outputs obtained from numerical simulations provide both physical insights and engineering guidance for the optimal design of Venturi-effect turbine arrays.

DOI: 10.6919/ICJE.202510_11(10).0006

4.1 Straight-Line Arrangement

In this subsection, five Venturi Effect Turbines are aligned according to a straight line, therefore the wake effect would be present, dampening power output. This arrangement is used to examine the significance of wake effect. Specifically, the tail-to-head distance has been varied to examine the strength of wake effect at different distances (behind a turbine). The following graphs represent simulation results at $D = D_1$; D_2 ; D_3 , respectively.

4.1.1 Velocity Reducing Wake Effects

As illustrated in Fig.3–Fig.5, the velocity fields of the straight-line arrangement clearly demonstrate the cumulative wake effect. The first turbine significantly reduces the centerline velocity downstream, creating an evident low-speed region within its wake. As the tail-to-head spacing increases from D_1 to D_3 , the wake region expands while the recovery of inflow velocity is slightly improved. Nevertheless, since all turbines are aligned along the same centerline, wake effects are transmitted consecutively in the streamwise direction, resulting in progressively lower inflow velocities for the downstream units and forming a distinct "deceleration chain" along the array.

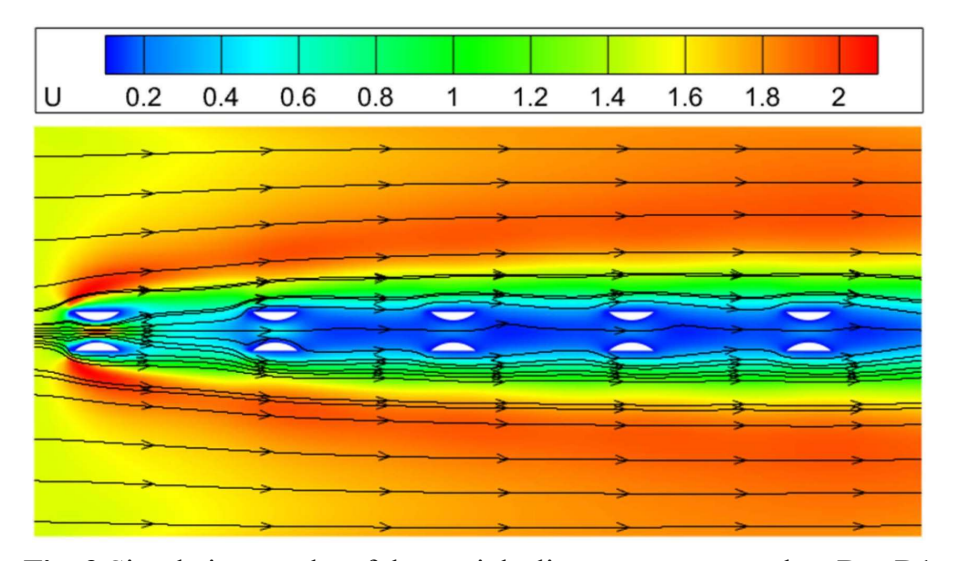


Fig. 3 Simulation results of the straight-line arrangement when D = D1

To further quantify this phenomenon, Fig.6–Fig.8 present the variation of inflow velocity with turbine ordinal position for different spacings. The results show that the velocity decreases with turbine position following a power-law decay, with high coefficients of determination $R^2 \approx 096-0.97$. For the smallest spacing D_1 , the fitted exponent reaches -1.336, and the inflow velocity of the downstream turbines drops rapidly to less than one-third of the freestream after the third unit, indicating the strongest wake superposition. When the spacing increases to D_2 and D_3 , the decay rate becomes less steep, with fitted exponents of -1.242 and -1.222, respectively. This trend suggests enhanced wake recovery between adjacent turbines, although the velocity deficit still persists.

In summary, the straight-line arrangement is characterized by strong velocity-reducing wake effects that substantially limit the energy capture of downstream turbines. Increasing the tail-to-head spacing can partially mitigate the velocity deficit, but it cannot eliminate the cumulative wake interaction, which funda-mentally constrains the total power output of straight-line arrays.

4.1.2 Total Power Output of Straight-Line Arrangement

The simulation assumes that all turbines are identical in size and operate at 100% efficiency. Accordingly, the combined power output of five turbines can be calculated using $P = \sum_{n=1}^{5} \rho A U_n^3$ Based on previous calculations, the area ratio is determined as $R_A = 0.53421$, which is adopted for all simulations.

Fig.9 illustrates the relationship between the total power output and the tail-to-head spacing in the straight-line arrangement. The results show that the total power increases slightly as the spacing grows from D_1 to D_3 , with values rising from approximately 6.55 kW to 6.73 kW. This gradual improvement is attributed to the partial recovery of inflow velocity between successive turbines, which alleviates the severe wake deficit observed at smaller spacings.

Nevertheless, the overall increase in power remains modest despite larger spacing, suggesting that the cumulative wake interaction inherent in the straight-line configuration fundamentally restricts the potential for efficiency enhancement. Therefore, while enlarging the tail-to-head distance can mitigate velocity losses to some extent, it cannot fully overcome the performance degradation induced by wake effects on downstream turbines.

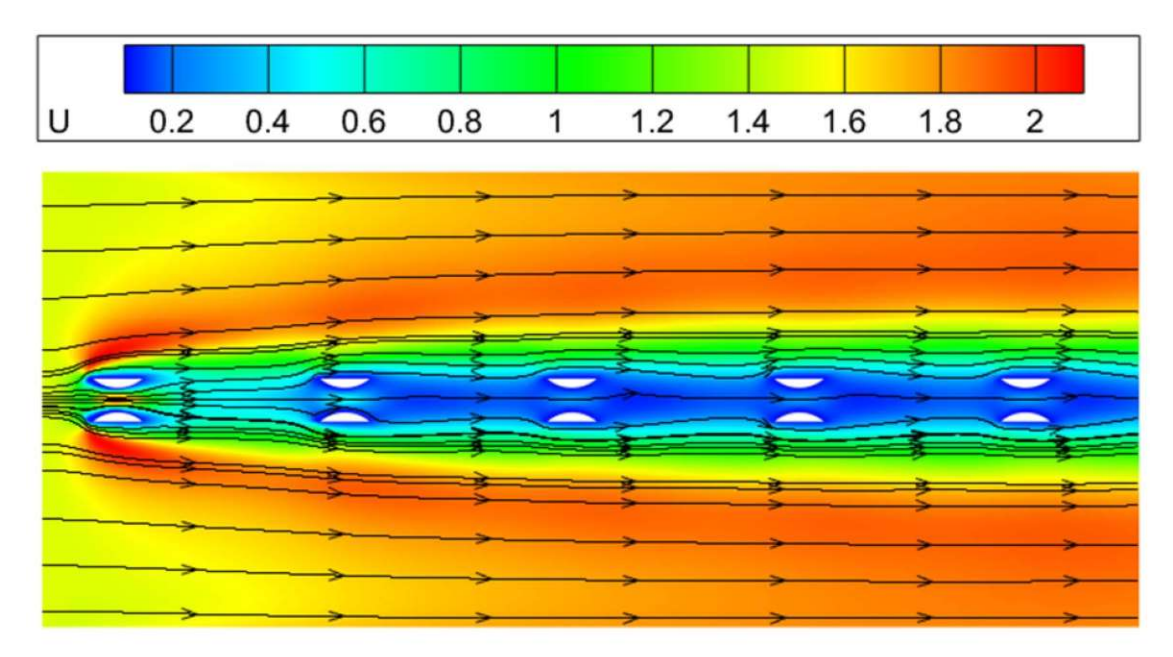


Fig. 4 Simulation Results of the straight-line arrangement when D = D2

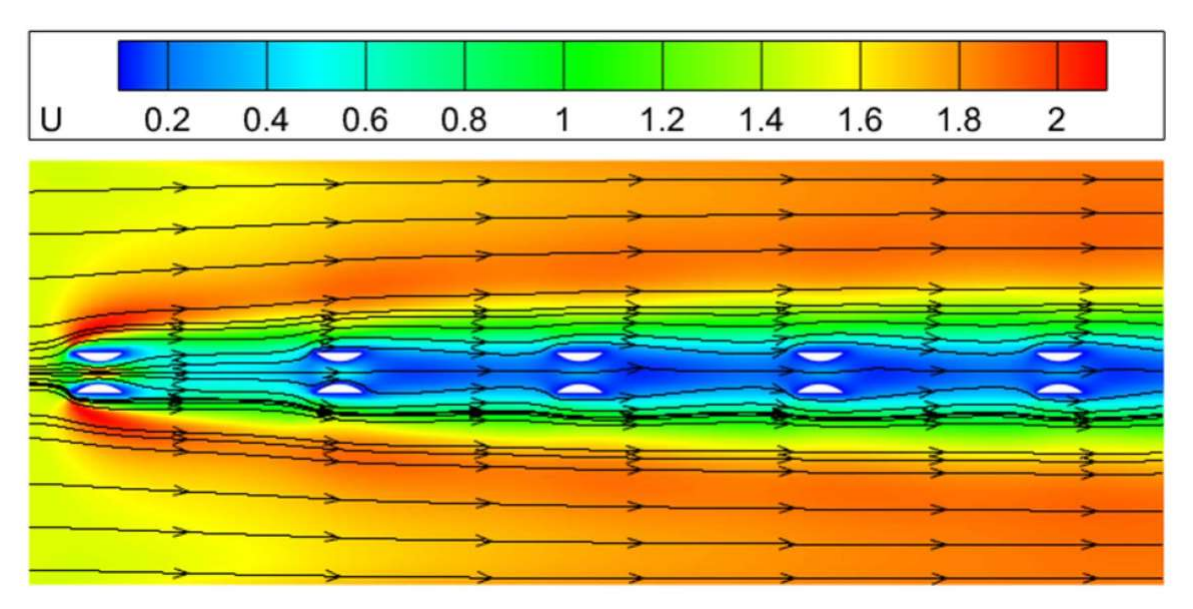


Fig. 5 Simulation Results of the straight-line arrangement when D = D3

ISSN: 2414-1895

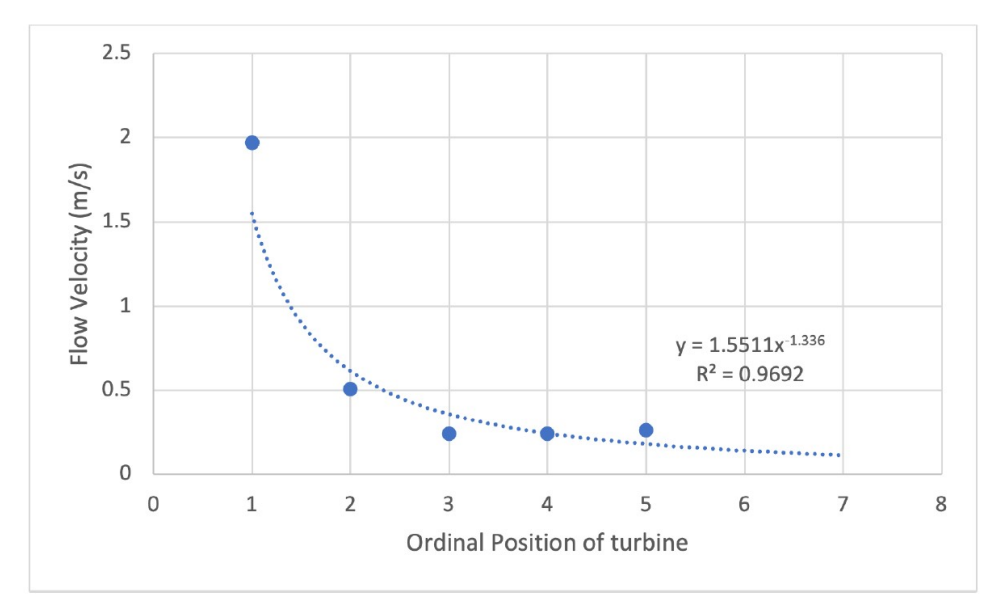


Fig. 6 Relationship between n and U_n when $D=D_1$

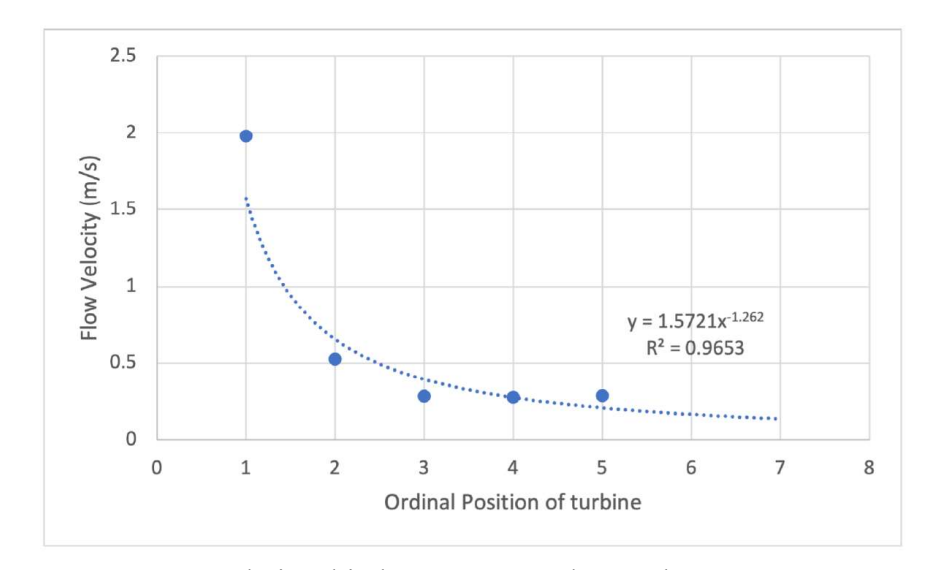


Fig. 7 Relationship between n and U_n when $D = D_2$

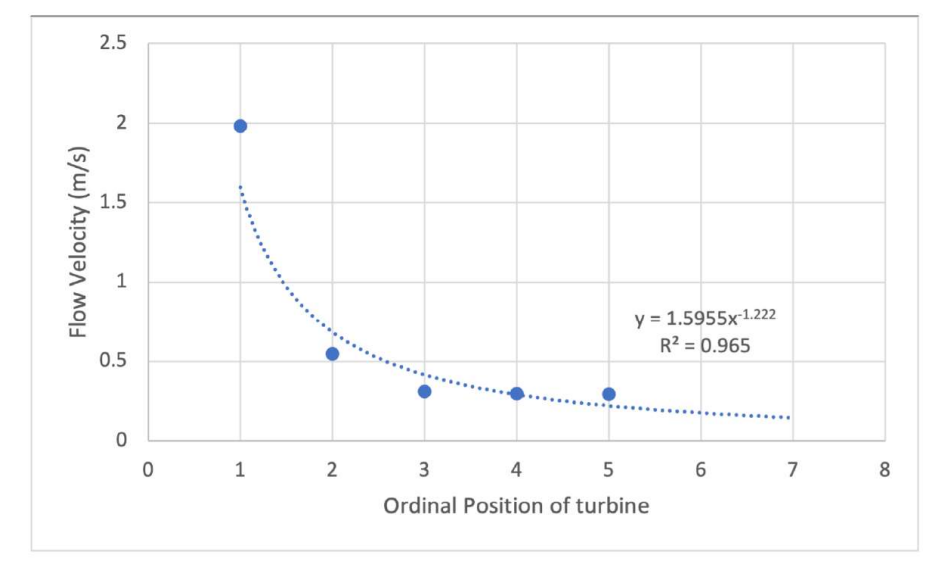


Fig. 8 Relationship between n and U_n when $D=D_3$

ISSN: 2414-1895

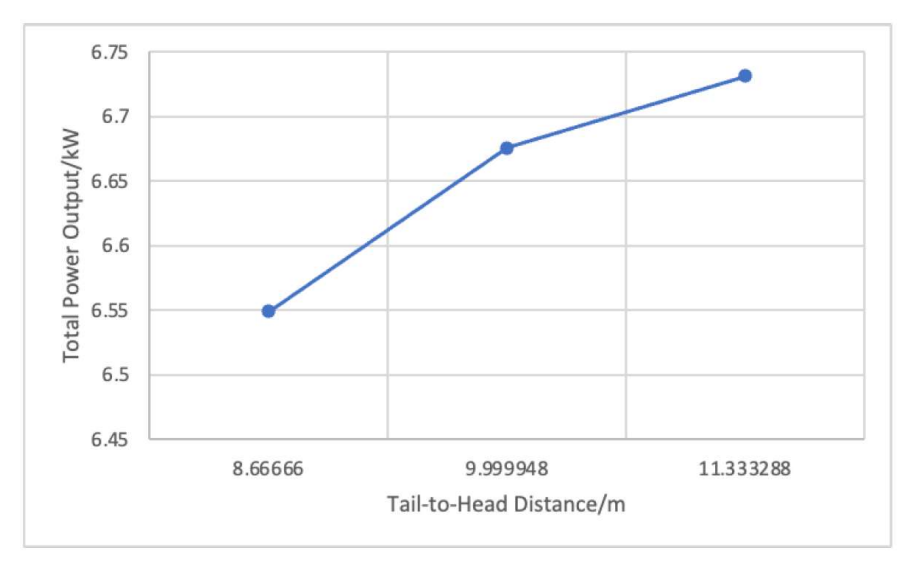


Fig. 9 Relationship between total power output and the tail-to-head distance between turbines with straight-line arrangement

4.2 Alternating Arrangement

The analysis of the straight-line configuration has demonstrated that cumulative wake interactions significantly reduce the inflow velocity of downstream turbines, thereby limiting the total power output of the array. To mitigate these adverse wake effects, an alternating arrangement is introduced, in which the second row of turbines is laterally shifted by half of the row spacing relative to the first row. This staggered configuration is expected to generate acceleration corridors between adjacent wakes, allowing downstream turbines to benefit from partially restored inflow velocities.

In this section, we investigate the velocity field and power output of the alternating arrangement under different tail-to-head spacings. The objective is to assess the extent to which the staggered layout alleviates velocity deficits and enhances the overall efficiency of the Venturi-effect turbine array, providing a direct comparison with the straight-line case.

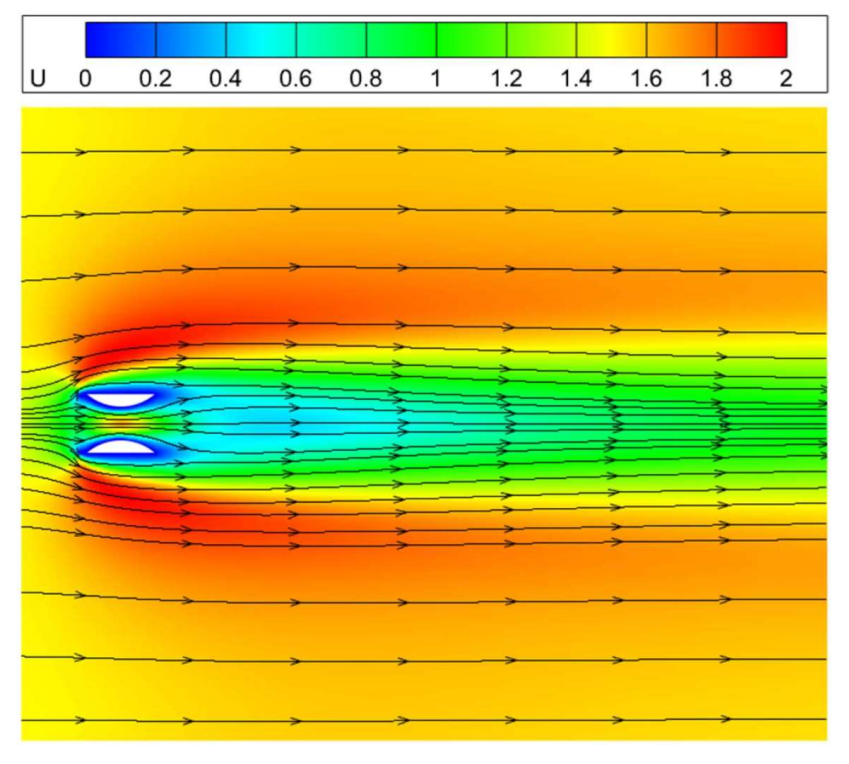


Fig. 10 Velocity field circumscribing one Venturi Effect turbine

ISSN: 2414-1895

4.2.1 Velocity Recovery in Alternating Layout

Fig.10 presents the velocity field surrounding a single Venturi-effect turbine, which highlights the formation of a low-velocity wake region downstream of the rotor. The velocity deficit is concentrated along the centerline and gradually recovers further downstream, while the lateral regions outside the wake remain largely unaffected. This single-turbine case establishes the baseline for evaluating wake development and its influence on subsequent turbines in an array. When turbines are arranged in an alternating layout, as shown in Fig.11–Fig.13, the wake characteristics differ significantly from the straight-line configuration. At the smallest spacing D_1 (Fig.11), the lateral offset between successive rows leads to the formation of acceleration corridors between adjacent wakes. These high-velocity pathways provide improved inflow conditions for downstream turbines, preventing them from being entirely engulfed by the wake of the upstream units. As the spacing increases to D_2 and D_3 (Fig.12 and Fig.13), the accelera-tion corridors become more pronounced and the extent of wake overlap is further reduced, thereby enhancing the recovery of centerline velocity and mitigating cumulative wake effects.

Overall, the alternating arrangement effectively redistributes the flow, generating regions of accelerated inflow that counteract wake-induced velocity deficits. This mechanism significantly improves the aerodynamic environment of downstream turbines compared with the straight-line case, laying the foundation for higher total power output in staggered arrays.

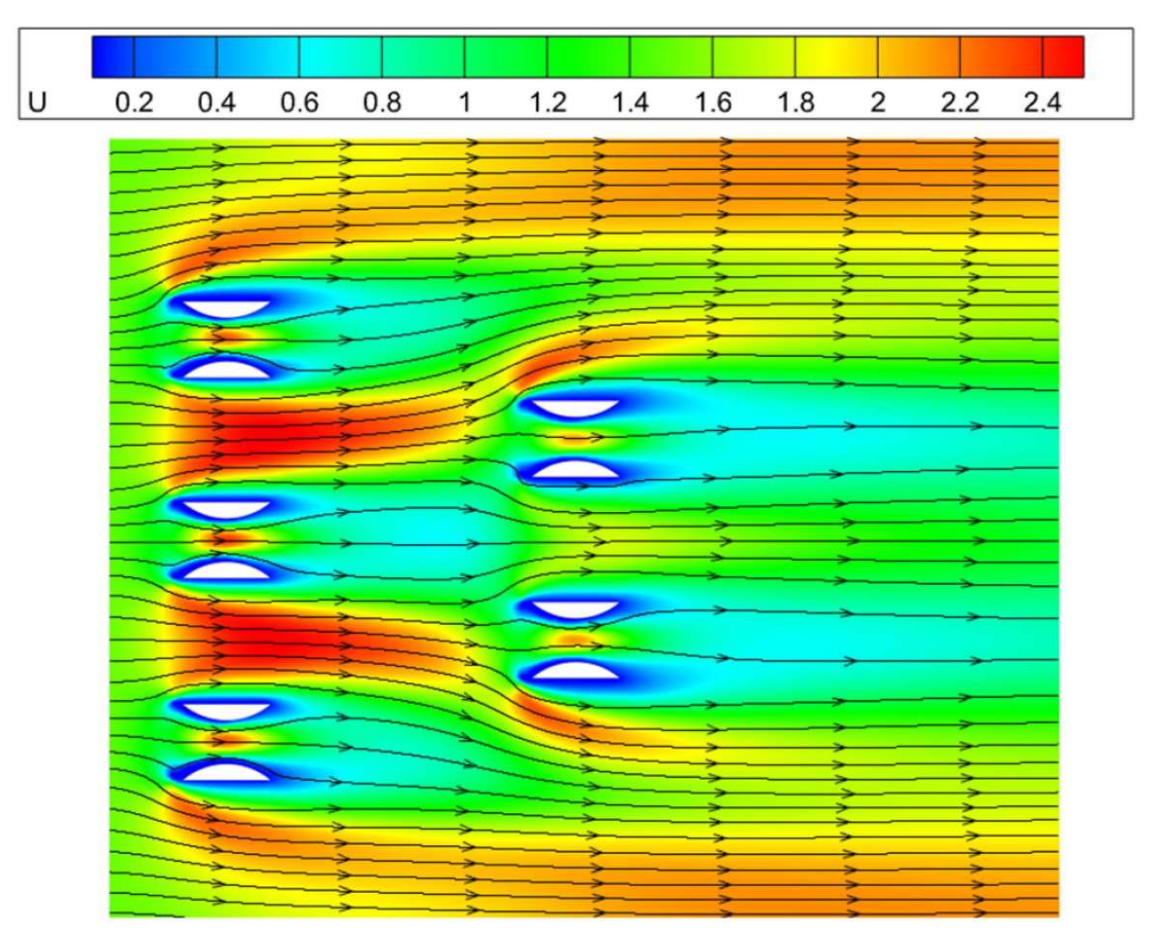


Fig. 11 Simulation results of the alternating arrangement when D = D1

ISSN: 2414-1895

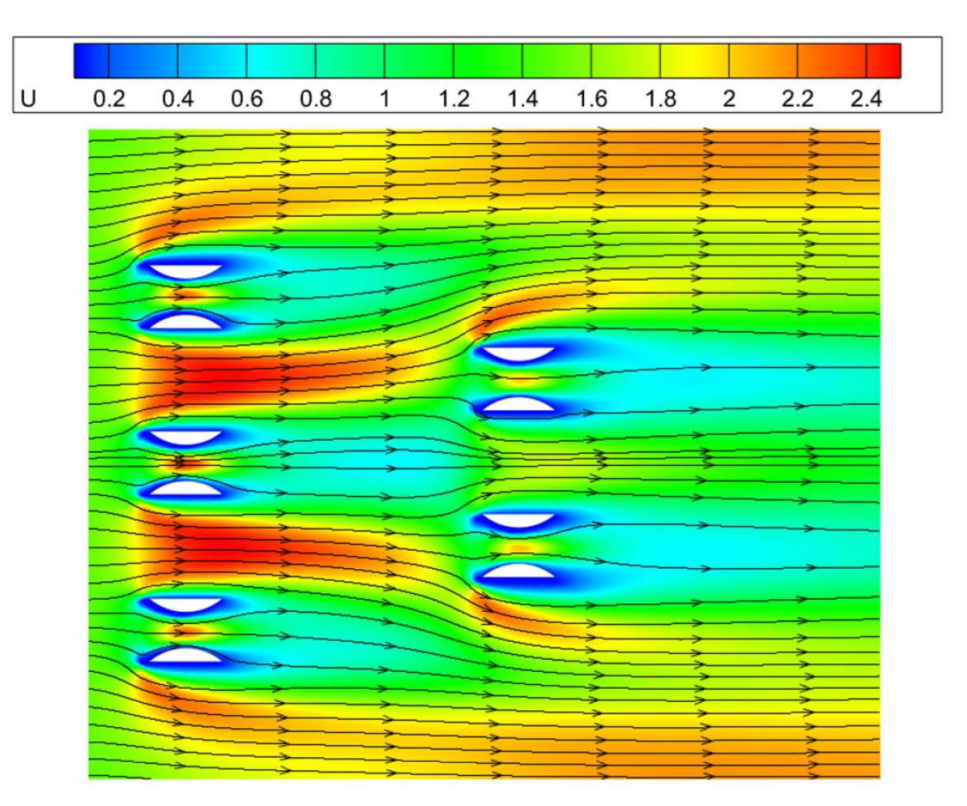


Fig. 12 Simulation results of the alternating arrangement when D = D2

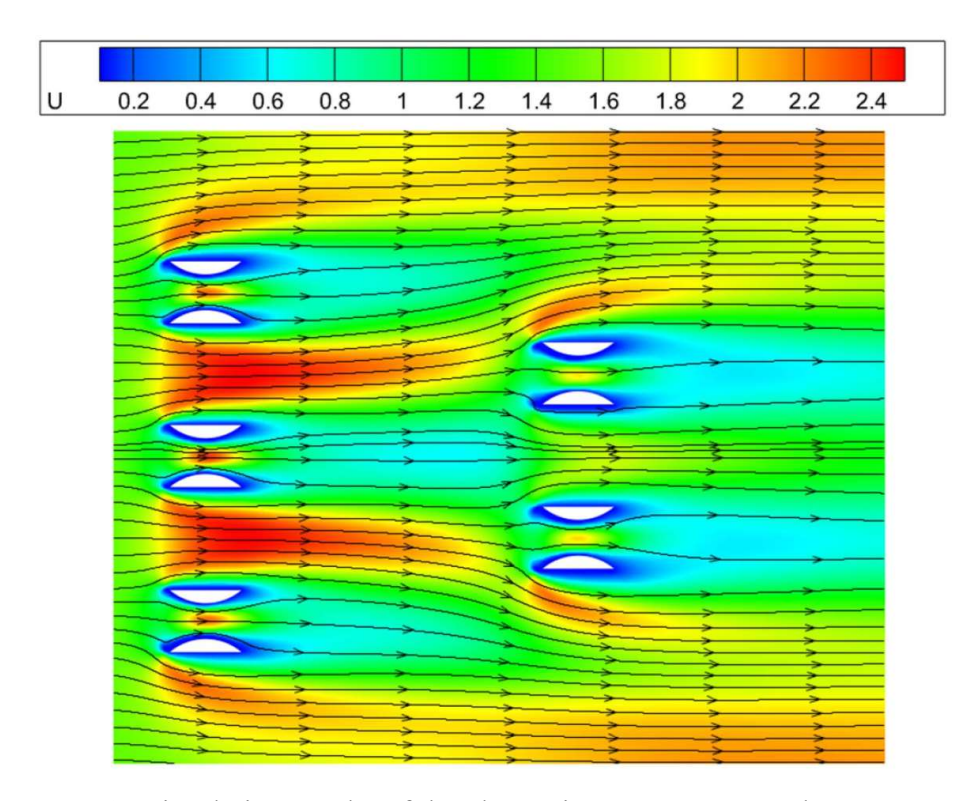


Fig. 13 Simulation results of the alternating arrangement when D = D3

4.2.2 Total Power Output of Alternating Arrangement

The staggered configuration not only alters the flow distribution but also leads to a markedly different trend in total power output compared with the straight-line case. As shown in Fig.11–Fig.13, the alternating layout generates acceleration corridors between successive rows, which substantially improve the inflow velocity of downstream turbines. This favorable redistribution of the flow enhances the contribution of each turbine to the overall array performance.

DOI: 10.6919/ICJE.202510_11(10).0006

Fig.14 presents the total power output of the alternating arrangement under different tail-to-head spacings. In contrast to the straight-line layout, where larger spacing slightly improves the array performance, the staggered configuration yields the highest total power at the smallest spacing D_1 (approximately 47.19 kW). As the spacing increases to D_2 and D_3 , the total power decreases steadily to about 44.01 kW. This reduction occurs because enlarging the spacing weakens the channeling effect of the staggered rows, diminishing the acceleration corridors that are most effective at short distances.

These results demonstrate that the alternating arrangement achieves superior energy extraction efficiency compared with the straight-line case, particularly when turbines are positioned with relatively small tail-to-head spacing. The staggered configuration thus provides a practical design strategy for maximizing the overall performance of Venturi-effect turbine arrays.

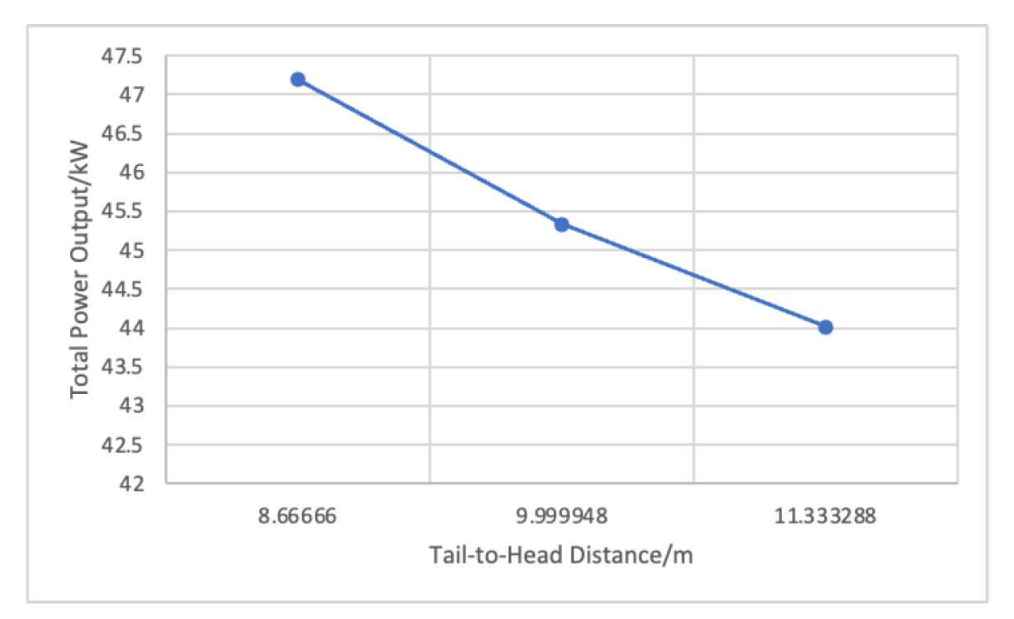


Fig. 14 Relationship between total power output and the tail-to-head dis-tance between turbines with alternating arrangement

4.3 Limitations of the Study

The present study is subject to several limitations that should be acknowledged. First, the analysis is conducted on a two-dimensional representation of the flow field, which only captures a cross-sectional view and may not fully reproduce the three-dimensional characteristics of the actual velocity distribution. This simplification, while computationally efficient, restricts the ability to capture complex flow interactions around the turbines. Second, the power estimation is based on the assumption that the velocity through the turbine cross-section is uniform, and the effects of the rotating blades are neglected. Consequently, the employed expression $P = 0.5\rho Au^3$ should be regarded as an approximation rather than an exact measure of turbine performance.

Furthermore, the Venturi-effect turbines are modeled using simplified geometric shapes to mimic contraction—expansion channels, which inevitably diverge from the detailed structures of practical turbine systems. While this abstraction is useful for isolating the effects of array configuration, it may not fully represent the operational performance of real devices. Finally, the conclusions are drawn from a limited set of simulation data, particularly with respect to the variation of tail-to-head spacing. Although the observed trends are consistent, additional data points would be required to construct more comprehensive and statistically robust trend lines.

These limitations highlight the need for future work to extend the analysis to three-dimensional models, incorporate realistic turbine geometries, and explore a broader parameter space to validate and refine the conclusions obtained in this study.

ISSN: 2414-1895 DOI: 10.6919/ICJE.202510_11(10).0006

5. Conclusion

While the straight-line arrangement of five Venturi Effect turbines illustrated the detrimental wake effects, and the alternating arrangement could, theoretically, suggest that the Venturi Effect engender an increase in power output for all of the turbines, the study deduced that, when constructing a series of underwater Venturi Effect turbines, incorporating an alternating arrangement is compulsory to ensure the overall efficiency of the turbines. Specifically, compared to the straight-line arrangement, incorporating an alternating arrangement can increase the total output by 701.0%. The study also pinpointed that, when considering the alternating arrangement, placing another column of turbines downstream that is closer to the column of turbines in front might yield an increase in total power output.

References

- [1] Randall, L.N., 1952. Rocket applications of the cavitating Venturi. J. Am. Rocket Soc. 22, 28–38.
- [2] Kumar, P., San, S.M., 2014. CFD study of the effect of Venturi convergent and divergent angles on low pressure wet gas metering. J. Appl. Sci. 14, 3036–3045
- [3] Ashrafizadeh, S.M., Ghassemi, H., 2015. Experimental and numerical investigation on the performance of small-sized cavitating venturis. Flow Meas. Instrum. 42, 6–15.
- [4] Sivakumar, M., Pandit, A.B., 2002. Wastewater treatment: a novel energy efficient hydrodynamic cavitational technique. Ultrason. Sonochem. 9, 123–131.
- [5] Arrojo, S., Benito, Y., 2008. A theoretical study of hydrodynamic cavitation. Ultrason. Sonochem. 15, 203–211.
- [6] Milly, P.J., Toledo, R.T., Harrison, M.A., Armstead, D., 2007. Inactivation of food spoilage microorganisms by hydrodynamic cavitation to achieve pasteurization and sterilization of fluid foods. J. Food Sci. 72, 414–422.
- [7] Ashokkumar, M., Rink, R., Shestakov, S., 2011. Hydrodynamic cavitation an alternative to ultrasonic food processing. Tech. Acoust. 9, 1–10.
- [8] Gogate, P.R., 2011. Hydrodynamic Cavitation for food and water processing. Food Bioprocess Technol. 4, 996–1011.
- [9] Carpenter, J., Badve, M., Rajoriya, S., George, S., Saharan, V.K., Pandit, A.B., 2016. Hydrodynamic cavitation: an emerging technology for the intensification of various chemical and physical processes in a chemical process industry. Rev. Chem. Eng. 33.
- [10] Gogate, P.R., Kabadi, A.M., 2009. A review of applications of cavitation in biochemical engineering/biotechnology. Biochem. Eng. J. 44, 60–72.
- [11] Gogate, P.R., Pandit, A.B., 2005. A review and assessment of hydrodynamic cavitation as a technology for the future. Ultrason. Sonochem. 12, 21–27.
- [12] Scardovelli, R., Zaleski, S., 1999. Direct numerical simulation of free-surface and interfacial flow. Annu. Rev. Fluid Mech. 31, 567–603.
- [13] Sadatomi, M., Kawahara, A., Kano, K., Ohtomo, A., 2005. Performance of a new microbubble generator with a spherical body in a flowing water tube. Exp. Therm. Fluid Sci. 29, 615–623.
- [14] Bashir, T.A., Soni, A.G., Mahulkar, A.V., Pandit, A.B., 2011. The CFD driven optimisation of a modified venturi for cavitational activity. Can. J. Chem. Eng. 89, 1366–1375.
- [15] Brinkhorst, S., von Levante, E., Wendt, G., 2016. Numerical investigation of effects of geometry on cavitation in Herschel Venturi-tubes applied to liquid flow metering. ISFFM #9.
- [16] Rudolf, P., Hudec, M., Gríger, M., Štefan, D., 2014. Characterization of the cavitating flow in converging-diverging nozzle based on experimental investigations. In: EPJ Web Conf. pp. 2101.
- [17] Vaz, J.R.P., de Lima, A.K.F., Lins, E.F., 2023. Assessment of a diffuser-augmented hydrokinetic turbine designed for harnessing the flow energy downstream of dams. Sustainability, 15(9), 7671.
- [18] Chawdhary, S., Angelidis, D., Colby, J., et al., 2018. Multiresolution large-Eddy simulation of an array of hydrokinetic turbines in a field-scale River: The Roosevelt Island Tidal Energy Project in New York City. Water Resources Research. 54(12), 10,188-10,204.

DOI: 10.6919/ICJE.202510_11(10).0006

- [19] Ouro, P., Nishino, T., 2021. Performance and wake characteristics of tidal turbines in an infinitely large array. J. Flu. Mech. 925: A30.
- [20] Ashrafizadeh, S.M., Ghassemi, H., 2015. Experimental and numerical investigation on the performance of small-sized cavitating venturis. Flow Meas. Instrum. 42, 6–15.
- [21] Jung, S.H., Seo, I. H., Kim, C. H. 2011. Effect of Venturi System on Acceleration of Low-speed Water Flow at the Venturi Throat Installed at the Inlet of Hydro Turbine. Journal of Advanced Marine Engineering and Technology (JAMET), 35(7), 914-920.